Available online at www.sciencedirect.com
ScienceDirect
Trans. Nonferrous Met. Soc. China 28(2018) 2214−2225
Transactions of Nonferrous Metals Society of China
www.tnmsc.cn

Effect of temperature on microstructure and texture evolution of Mg−Zn−Er alloy during hot compression

Jin-xue LIU[1], Ke LIU[1], Wen-bo DU[1], Shu-bo LI[1], Zhao-hui WANG[1], Xian DU[1], Cui-cui SUN[2]

1. College of Materials Science and Engineering, University of Technology Beijing, Beijing 100124, China;
2. Shandong Academy of Science, Ji'nan 250014, China

Received 1 June 2017; accepted 7 May 2018

Abstract: The microstructure and texture evolutions in Mg−Zn−Er alloy during hot compression were investigated by using optical microscope (OM), field emission scanning electron microscope (EBSD) and transmission electron microscope (TEM). The results indicate that the temperature plays an important role in dynamic recrystallization (DRX) mechanism. The twin dynamic recrystallization (TDRX) is induced at a strain of 0.6 because of the activation of non-basal slip $\langle a+c\rangle$ dislocations at 200 °C. Meanwhile, the continuous DRX (CDRX) occurs at 350 °C, which is identified by the typical necklace-like structure around the residual initial grains. The DRX contributes to the modification of texture significantly. The tension twins are responsible for the weak texture at 200 °C. Meanwhile, the decrease in the basal texture is ascribed to the DRX sites which transfer from twin boundaries to initial grain boundaries as the temperature is increased from 200 to 350 °C.

Key words: Mg−Zn−Er alloy; hot compression; dynamic recrystallization; twinning; texture

1 Introduction

As one of the lightest structural materials, the magnesium alloy has attracted more attention because of an emphasis on improving the use efficiency of fuel [1−3]. However, the formability of the magnesium alloy is so inferior in plastic deformation that its application for industry is restricted. The inferior plastic deformation is ascribed to the hexagonal close packed (HCP) structure and limited basal slip systems. As a result, the catastrophic failure occurs with little reduction during 2-D/multiracial stresses at low temperature. ANDO et al [4] reported that the interaction between the localized shear deformations and the $\{10\bar{1}1\}-\{10\bar{1}2\}$ double twins caused this catastrophic failure. Therefore, in order to improve the formability of the magnesium alloy, lots of thermal mechanical processing methods were carried out such as hot extrusion (HE), hot rolling (HR) and hot forging (HF).

During hot deformation, the dynamic recrystallization (DRX) often occurred, which provided an effective way to modify the texture and refine the grains. As reported, the mechanisms of DRX mainly included twin stimulated DRX (TDRX), continuous DRX (CDRX) and discontinuous DRX (DDRX) [5−7]. The nuclei of grains induced by the TDRX were usually activated at a low temperature because of the mutual intersection of the primary twins and the second twins within the primary twin lamellas [6,7]. Meanwhile, the formation of nuclei of CDRX grains was caused essentially by dislocation pile-ups and dislocation rearrangements with strain in primary grains at elevated temperature, and the new developing grains were nucleated evenly throughout the material [5,6]. In addition, the process of grain nucleation introduced by DDRX was caused by local migration of initial boundary developing a "bulge" and then the boundary was cut off by dislocations from grains at high temperature [5]. The different DRX mechanisms would have different impacts on the performance of magnesium alloys.

Lots of researches showed that formability and mechanical properties were related with the twin types (tension and compression twins), twin generation (primary or second) and deformation bands [7−11]. The double twins had a great influence on DRX, shear bands

Foundation item: Project (2172013) supported by the Natural Science Foundation of Beijing, China; Project (2016YFB0301101) supported by the National Key Research and Development Program, China; Project (KZ201810005005) supported by Key Science and Technology Program of Beijing Municipal Commission of Education, China
Corresponding author: Ke LIU; Tel/Fax: +86-10-67392917; E-mail: lk@bjut.edu.cn
DOI: 10.1016/S1003-6326(18)64866-6

and compression twins [12,13]. In addition, the strong basal texture generally formed during hot deformation, and it reduced the ductility of magnesium alloys [2]. Therefore, the modification of texture is necessary to improve the mechanical properties of magnesium alloys.

As mentioned above, the temperature has a significant effect on DRX and modification of the texture. It was well known that magnesium alloys containing rare earth (RE) elements showed high yield tensile strength, low anisotropy and random texture, compared with RE-free magnesium alloys. Thus, it is important to investigate the evolutions of both microstructure and texture during hot plastic deformation with temperature. In our previous investigation, we found that the deformation temperature was a key factor to decide the kinds of DRX mechanisms [14]. However, most researches on the DRX, twining and texture in Mg−Zn−RE alloys were mainly focused on deformation temperature during hot extrusion/rolling. There was few report on the relationship between the DRX/twins and the texture in Mg−Zn−RE series alloys at different temperature. Thus, the present study aims to investigate the DRX and twins so as to elucidate their influence on microstructure and texture evolutions of the Mg−Zn−Er alloy during hot plastic deformation at both low (200 °C) and high (350 °C) temperature.

2 Experimental

The Mg−4.5Zn−0.75Er alloy was prepared from pure Mg (99.99%, mass fraction), pure Zn (99.99%, mass fraction) and Mg−30%Er (mass fraction) master alloys in a graphite crucible with an electric resistance furnace under an anti-oxidizing flux. The chemical composition of the alloy was analyzed by using X-ray fluorescence (XRF) analyzer to be Mg−4.50%Zn−0.726% Er (mass fraction). The as-cast alloy was solution-treated at 460 °C for 20 h followed by quenching into water. The as-solution-treated alloy had homogeneous and equiaxed grains with a mean grain size of ~200 μm, as shown in Fig. 1(a). The as-solution-treated alloy had a relatively random distribution of basal and prismatic planes, and the maximum intensity of the random texture was ~15.44, as shown in Fig. 1(b).

The as-solution-treated alloy was machined into 10 mm in diameter and 15 mm in height for compression tests. The longitudinal direction of the cylinders was parallel to the compression direction. The compression test was carried out on the Gleeble−1500 thermo-mechanical simulator and the stress−strain curves were obtained. The samples were compressed to the total true strain of 0.08, 0.15, 0.45 and 0.6 at 200 °C and 350 °C, respectively, with strain rate of 1 s^{-1} and then quenched into water.

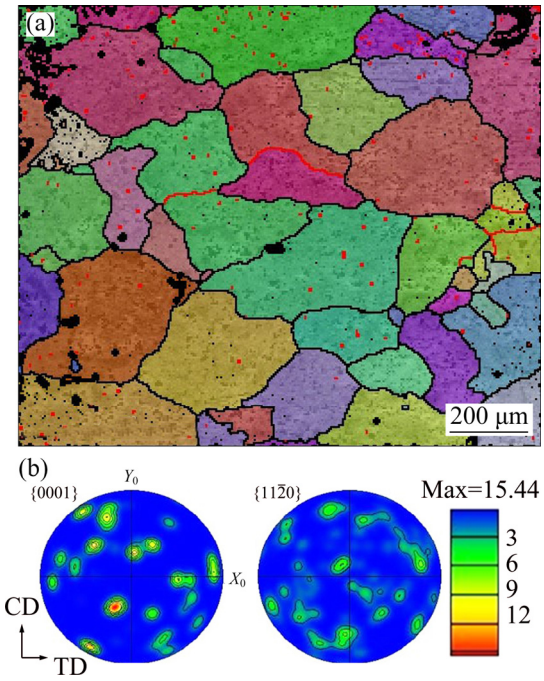

Fig. 1 Inverse pole figure map (a) and pole figures (b) of solution-treated Mg−4.5Zn−0.75Er alloy

The as-compressed specimens were cut along the compression direction in order to observe the microstructure and texture evolutions. The microstructure and crystallographic orientation were analyzed by OM and EBSD, respectively. Additionally, the deformation twins and DRXed grains formed in the as-compressed Mg−Zn−Er alloy were systematically analyzed by using TEM and EBSD, respectively. The samples for OM observation were mechanically polished and etched in a solution of 4 mL nitric acid and 96 mL ethanol. Samples for EBSD analysis were prepared by electro-polishing with a solution of 60% methanol, 30% glycerol and 10% nitric acid at 25 °C (voltage of 10−15 V) for 10−15 s. Besides, the samples were prepared for the EBSD observation by sectioning and polishing, and the plane for EBSD observation was along the compression direction (CD) and the transverse direction (TD). The specimens for TEM observation were prepared by cutting, grinding and argon ion-beam thinning at an angle incidence less than 10°.

3 Results and discussion

3.1 Stress−strain curves of Mg−Zn−Er alloy

Figure 2 shows the true stress−strain curves of the specimens at 200 and 350 °C with a strain rate of 1 s^{-1}. At 200 °C, the flow stress does not reach a steady state. Moreover, an instable state is observed on the true stress−strain curve at 200 °C due to the stress concentration as the strain increases. At 350 °C, the

stress increases with the increase of strain, and the stress reaches a maximum value when the strain is ~0.15. As the strain increases further, the stress begins to decrease. Moreover, when the strain is increased to 0.45, the flow curve is already in a steady state. In addition, it is found that the stress decreases obviously at different strains when the temperature increases from 200 to 350 °C.

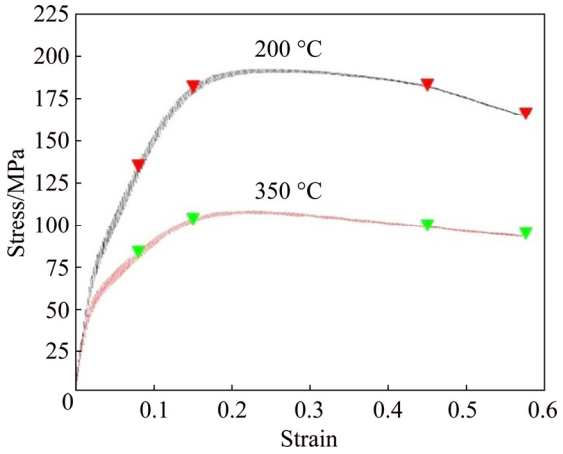

Fig. 2 True stress−strain curves of Mg−4.5Zn−0.75Er alloy at 200 and 350 °C

3.2 OM images of Mg−Zn−Er alloy

Figure 3 shows the OM images of the Mg−4.5Zn−0.75Er alloy after compression with different strains at 200 °C. A certain amount of cross-cutting twins are found and the size of twins decreases as the strain increases, as shown in Fig. 3. The {0001} basal slip and twinning are considered as main deformation mechanisms for magnesium alloys during plastic deformation at room/low temperatures [15−17]. At the beginning of deformation process, the twining plays a great important role in modifying the ductility of magnesium alloys via rotating the basal plane towards a more favorable orientation [11]. However, as the strain increases, the formation of twin boundaries hinders the movement of dislocations, which results in stress concentration [13]. The narrower twin slices stand for severer stress concentration, which indicates that the stress is not released in time. As a result, the morphology containing stepped structures forms as the strain reaches up to 0.45, as shown in Fig. 3(c). Furthermore, the increase in strain (about 0.6) activates the DRX, and some fine recrystallized grains are observed in twin lamellae, as seen in Fig. 3(d). The twin lamellae full of fine recrystallized grains further develop into shear bands via consuming twin layers. The shear bands generally appear in dark streamlines and about 40° tilting to compression direction (CD).

Figure 4 shows OM images of the Mg−4.5Zn−0.75Er alloy after compression with different strains at 350 °C. At a strain of 0.08, there exist a number of lentoid twins in this alloy, which indicates that the twinning is still one of the main deformation modes. At a strain of 0.15, the twin is still present. At the same time, a number of fine recrystallized grains are found in

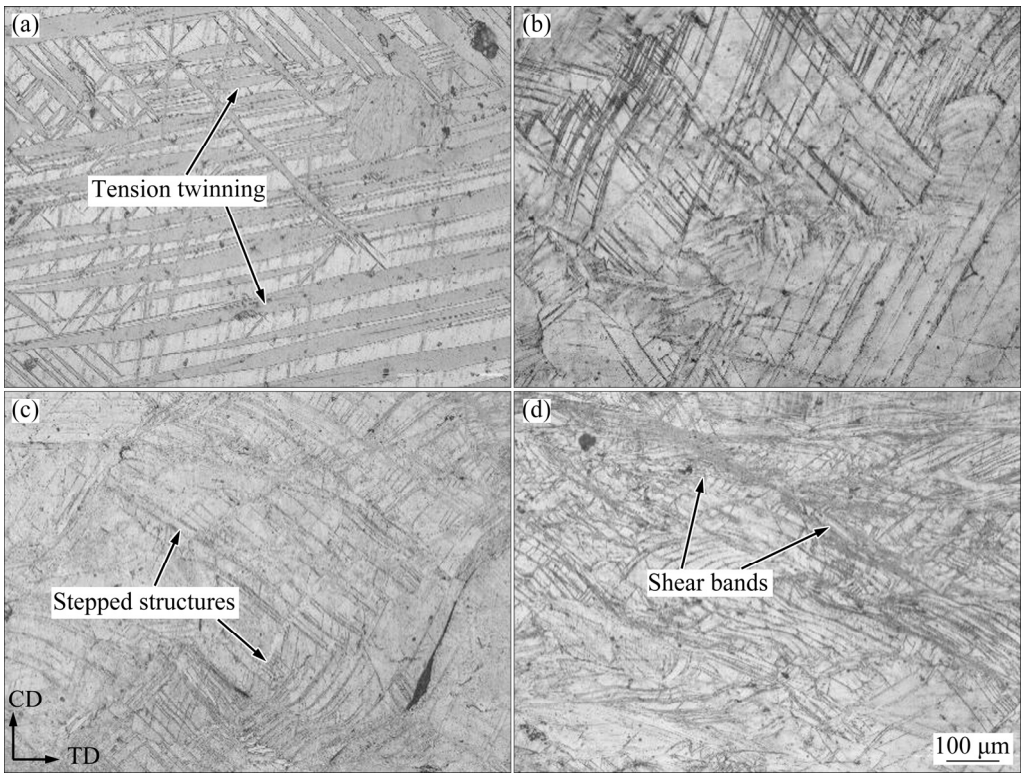

Fig. 3 Optical images of as-compressed Mg−4.5Zn−0.75Er alloy at 200 °C with different strains: (a) 0.08; (b) 0.15; (c) 0.45; (d) 0.60

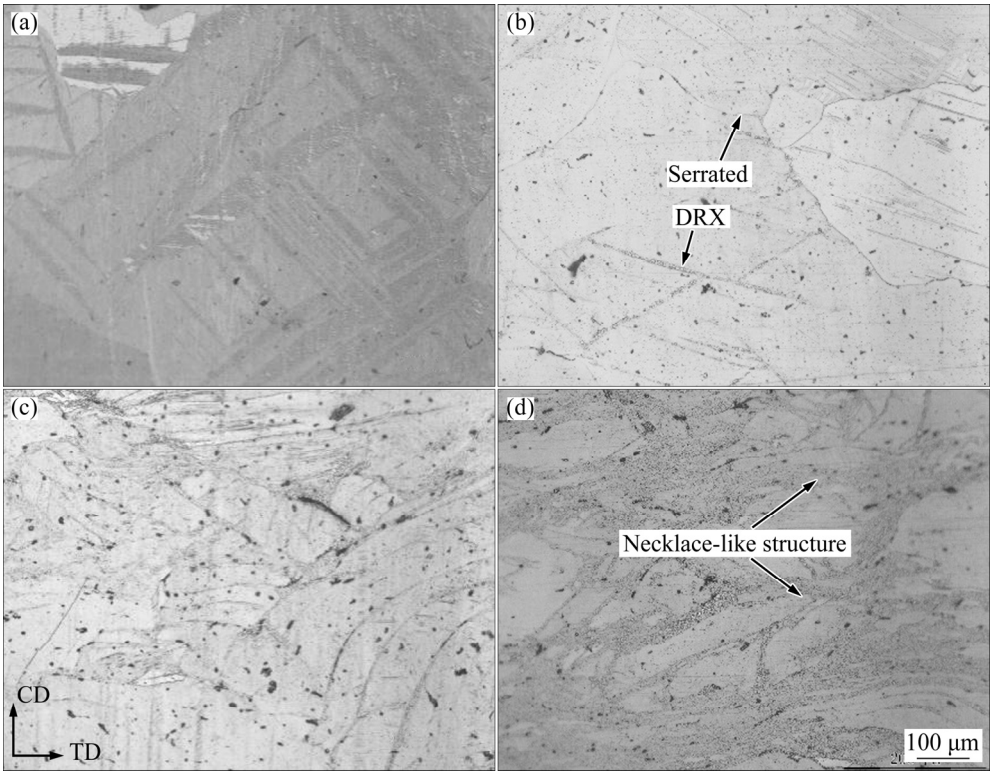

Fig. 4 Optical images of as-compressed Mg−4.5Zn−0.75Er alloy at 350 °C with different strains: (a) 0.08; (b) 0.15; (c) 0.45; (d) 0.60

necklace-like structure at both original boundaries and twin boundaries, as shown in Fig. 4(b). It is suggested that the occurrence of DRX is related not only with the temperature but also with the strain [7]. Furthermore, the DRX begins to occur at grain boundaries even in the interior of grains at the strain of 0.6. The DRX is initiated at grain boundaries and twin boundaries, which is closely related with dislocations pile-up and rearrangement under the strain localization [18]. Although the nucleation rate increases under the relatively high strain rate of 1 s^{-1}, the recrystallized grains are still fine because of short deformation time.

3.3 Microstructure evolutions of Mg−Zn−Er alloy

The microstructure evolutions of the Mg−4.5Zn−0.75Er alloy after compression were investigated by using EBSD. The inverse pole figures (IPF), grain boundary angle distribution graphs and image quality (IQ) maps with twin distribution observed from specimens after compression at 200 °C with strains of 0.08, 0.15, 0.45 and 0.6 are shown in Fig. 5. Notably, plastic strain in the lattice makes Kikuchi lines blurred. The quantity of Kikuchi patterns can be directly reflected in IQ maps, which allows for qualitative analysis on stress and strains. The low IQ means that there exists large stress and strains in the interior of specimens, which results in the formation of incomplete lattices, numerous dislocations and other defects. It is obviously observed that the IQ is very high at strains of 0.08 and 0.15. Conversely, it is low at other strains. Accordingly, the main types of twins and microstructures have changed due to the influence of stress and strain. The as-compressed specimen mainly consists of twins at a strain of 0.08 (Fig. 5(c)). The twins distribution figure indicates that the type of twins is mainly the $\{10\bar{1}2\}$ extension twin (86.3°) [19]. Besides, some second tension twins form inside the primary tension twins, which is ascribed to the rotation of twin axis in the primary twin at a relatively low strain.

Meanwhile, the average size of extension twins decreases when the strain is increased to 0.15. The twin types have also changed, and a small number of $\{10\bar{1}1\}$, $\{10\bar{1}3\}$ contraction twins as well as $\{10\bar{1}1\}-\{10\bar{1}2\}$ double twins are present, as shown in Figs. 5(d) and (f). Moreover, a few of low angle grain boundaries (2°−15°, LABs) are also found, as seen in Fig. 5(e). The LABs are dislocations accumulated within the as-deformed structure, which indicates the stored energy in metals after plastic deformation [20]. At a strain of 0.45, the extension twins disappear, which are replaced by contraction twins and double twins, as shown in Figs. 5(g)−(i). However, both the contraction twins and double twins are so narrow that they cannot coordinate the deformation during the hot compression. Meanwhile, the critical resolved shear stress (CRSS) for prismatic $\langle a \rangle$ slip and pyramidal $\langle a+c \rangle$ slip is much higher than that of the basal slip at low temperature, which cannot lead to

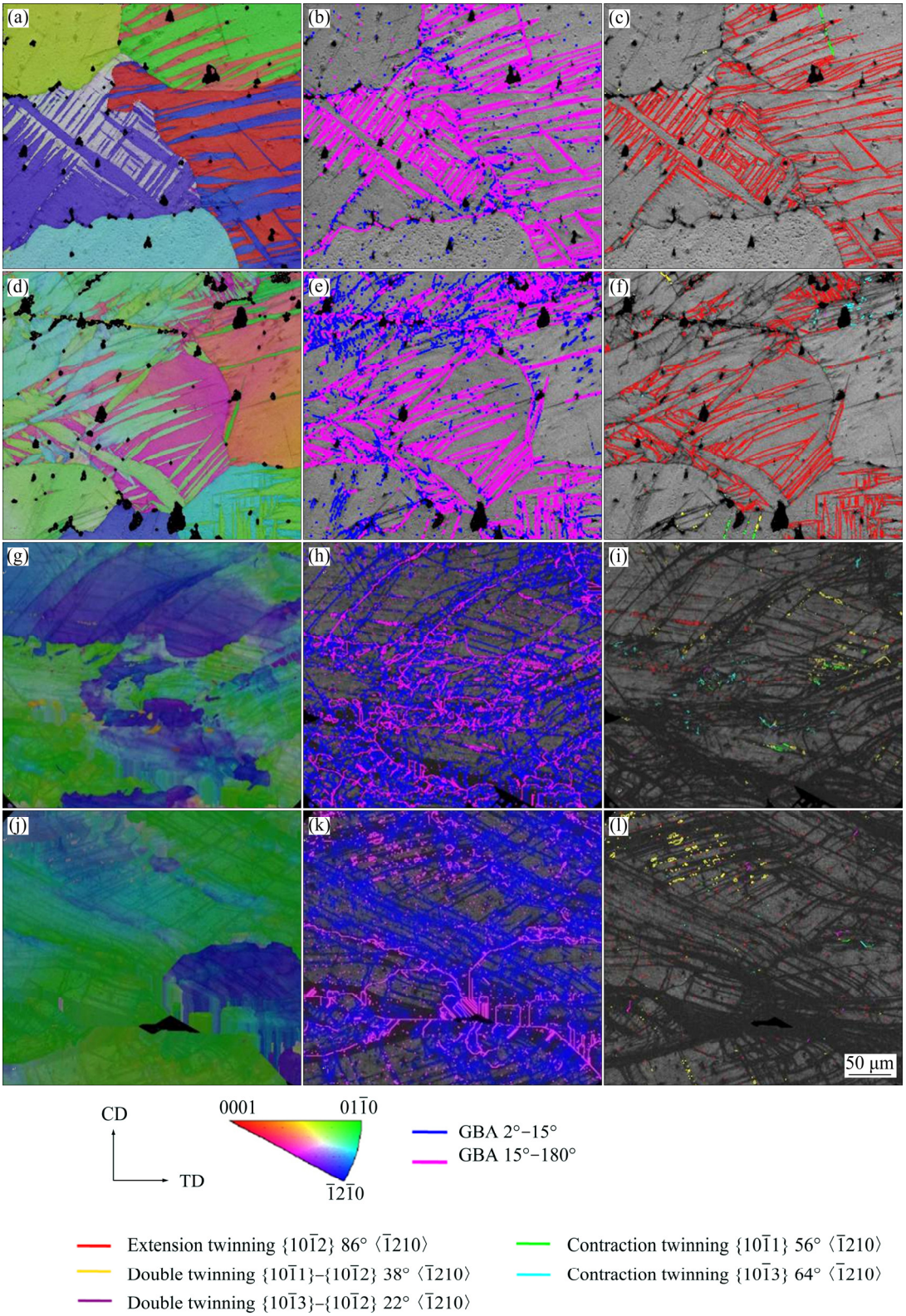

Fig. 5 Inverse pole figures (a, d, g, j), grain boundary angle distribution figures (b, e, h, k) and twin distribution figures (c, f, i, l) of as-compressed alloy at 200 °C with different strains: (a−c) 0.08; (d−f) 0.15; (g−i) 0.45; (j−l) 0.60

the activation of non-basal slips [21]. Consequently, the surface steps form, and the stress concentration is eliminated, as shown in Fig. 3(c). When the strain is increased from 0.45 to 0.6 (Fig. 3(d), Figs. 5(j)−(l)), the fractions of low angle grain boundaries and double twin boundaries increase obviously. It is indicated that the sub-structures and DRX grains have already been generated. The microstructures of the as-compressed

alloy mainly contain $\{10\bar{1}1\}-\{10\bar{1}2\}$ double twins and shear bands. Moreover, the formation of the sub-structure is related with the contraction twins and double twins, which are responsible for the formation of shear bands [22,23].

In order to further investigate the twin types and DRX mechanisms, the TEM observation of the as-compressed alloy at 200 °C was carried out. Figure 6(b) indicates that double twin lamellae of ~0.7 μm is observed at the strain of 0.15, the type of which is $\{10\bar{1}1\}-\{10\bar{1}2\}$ according to EBSD analysis (Fig. 5(f)) [7,24]. Compared with the relatively high density of dislocations, the higher density of dislocation clusters and rearrangement constitute the dislocation walls in contraction twins at the strain of 0.45, as shown in Fig. 6(c). As mentioned above, the formation of twin bands (a set of parallel and symmetrical $\{10\bar{1}1\}$ compression twin lamellae) results in ineffective release of stress via formation of contraction twins and double twins. The twin bands continue to trapping dislocations, which can generate a great deal of dislocation walls, second twins, double twins and even micro-twins in the second twins (as shown in Figs. 6(c) and (d)). Moreover, as the strain is increased up to 0.6, a significant number of sub-grains are formed, which is ascribed to the accumulation of stress. The accumulation of stress induces the activation of the non-basal slip $\langle a+c\rangle$ dislocations inside the twin bands and around the twin boundaries.

The above phenomena of these three kinds of twin nucleation processes are recognized as the features of the TDRX mechanism [6,7]. The schematic illustration of the twin DRX nucleation in twin bands is shown in Fig. 7. As seen in Fig. 7(a), in the twin bands, the dislocations pile up in interiors of twins. The dislocation walls are formed by rearrangement at a certain angle with primary twins, and then the subsequent dislocations assist the walls to migrate locally in order to reduce their stored energy. Consequently, the deformation twin is subdivided into nuclei by the development of transverse low-angled boundaries [6]. Figure 7(b) shows $\{10\bar{1}1\}-\{10\bar{1}2\}$ double twin which is the second $\{10\bar{1}2\}$ twin occurring in the primary $\{10\bar{1}1\}$ twin. As reported, the basal slip dislocations move across the $\{10\bar{1}1\}$ twin and pile up at the $\{10\bar{1}2\}$ twin boundaries in double twins, resulting in the formation of low-angle boundaries inside or near double twins [7]. The second twins and micro-twins within primary twin lamellae are

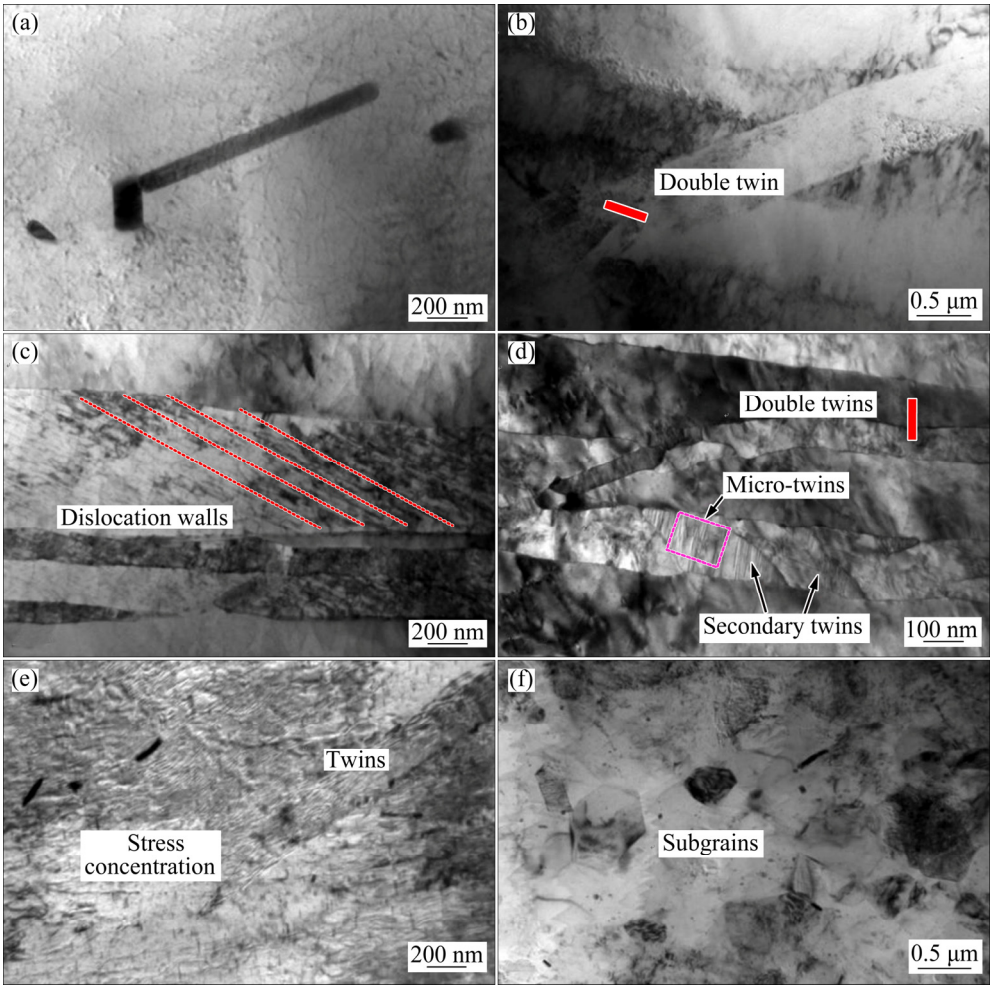

Fig. 6 TEM images of as-compressed alloy at 200 °C with different strains: (a, b) 0.15; (c, d) 0.45; (e, f) 0.60

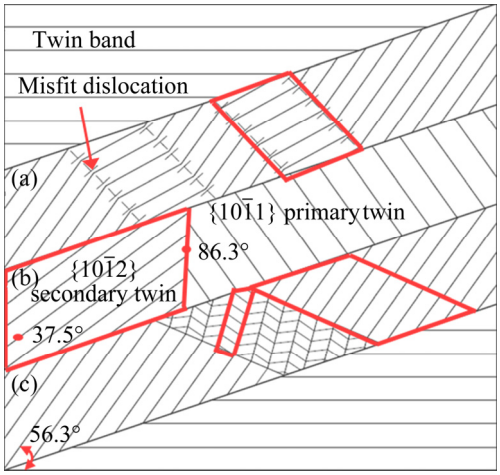

Fig. 7 Schematic representation of twin DRX mechanism at 200 °C (red parallelogram regions show nuclei): (a) Nucleation by subdivision of primary twin lamellae and low-angle boundaries; (b) Nucleation by subdivision of primary {10$\bar{1}$1} twin by second {10$\bar{1}$2} tension twin; (c) Nucleation by subdivision of primary twin lamellae by fine second twins and micro-twins

shown in Fig. 7(c). Similar to Fig. 7(b), the formation of the nuclei is related with both the basal slip ⟨*a*⟩ dislocations and the non-basal slip ⟨*a*+*c*⟩ dislocations, which are pinned by the twin-walls during the formation of the micro-twin boundaries and the second twin boundaries [25]. The critical resolved shear stress (CRSS) for the activation of the non-basal slip ⟨*a*+*c*⟩ dislocations is so high at room temperature that the distortion is needed to be further accumulated via dislocation pile-ups at a strain of 0.6. The sub-grains can form via three kinds of TDRX mechanisms and gradually transform into random boundaries by absorbing more dislocations due to an additional increase in misorientations within matrix. However, the TDRX grains cannot grow up because of the poor grain boundary migration under the condition of low temperature. Since the grain boundary migration depends on temperature, it is a rate-controlling process. The DRX occurs at 200 °C and exhibits obvious strain rate sensitivity [25]. The shear bands begin to form while the twin bands are consumed via the formation of ultrafine TDRX grains in the present investigation [22]. In other words, the shear bands can be defined as streamlined strips, which are composed of broken twins (compression and double twin lamellae) and tiny TDRX grains.

Figure 8 shows the EBSD maps of the specimens after compression at 350 °C. The microstructure mainly includes twins at a small strain of 0.08, and the type of the twins is {10$\bar{1}$2} extension twin, as shown in Fig. 8(c). According to the previous research [20], the number of ⟨*a*+*c*⟩ non-basal slip dislocation is large at low temperature and drops rapidly as the temperature increases whereas the twinning is relatively insensitive to the temperature. Therefore, compared with that at 200 °C, the number of twins decreases because the plasticity capability is developed by activation of non-basal slips at 350 °C (as seen in Fig. 3(a) and Fig. 4(a)). In addition, some low-angle grain boundaries appear (as seen in Fig. 8(b)), resulting from the accumulation of a large number of ⟨*a*+*c*⟩ slip and ⟨*a*⟩ slip dislocations near the twin boundaries and grain boundaries.

With the development of the deformation degree, the migration ability of twin boundary is improved gradually as well as the interaction between twin boundaries and dislocations, which results in a transformation from twin boundaries into random grain boundaries [26]. Hence, when the strain is up to 0.15, the DRX occurs at both the twin boundaries and initial grain boundaries (Fig. 8(d)). In the meantime, the number of extension twins dwindles by the recrystallization, as shown in Fig. 8(f). It is well indicated that the severer deformation is, the more grain refinement will be via the dynamic recrystallization at intermediate and high temperatures. Consequently, as the strain is increased to 0.45, the number of low-angle grain boundaries further increases while the twins nearly disappear, as seen in Figs. 8(g)−(i). It is obviously found that the number fraction of boundaries with misorientation angles less than 15° decreases while the number fraction of boundaries larger than 15° increases with the strain increasing from 0.45 to 0.60, as indicated in Figs. 8(j)−(l). It is suggested that the substructure with low-angle grain boundaries around initial grain boundaries absorbs subsequent dislocations and then develops into fine grains with high-angle boundary during compression, which is considered as a CDRX process [5,6,19,27−29]. The CDRX mechanism has been described by SITDIKOV and KAIBYSHEV [6], and VALLE et al [27].

In the initial stage of nucleation, the interaction between non-basal dislocation slips and cross slips leads to the formation of dislocation cells at both mantle regions of initial grains and twin boundaries. Then, the formation of sub-grain boundaries takes place by extended recovery. Ultimately, the high angle boundaries form via sub-boundary migration and coalescence. In order to further investigate the CDRX mechanism of the alloy during compression at 350 °C, the TEM images of the specimen are shown in Fig. 9. Plenty of pile-up and tangling dislocations around grain boundaries are observed. It is indicated that the dislocation cells transform from dislocations tangling, and then gradually develop into sub-grains at strain of 0.15 (as shown in Figs. 9(a) and (b)). As a result, serrated grain boundaries

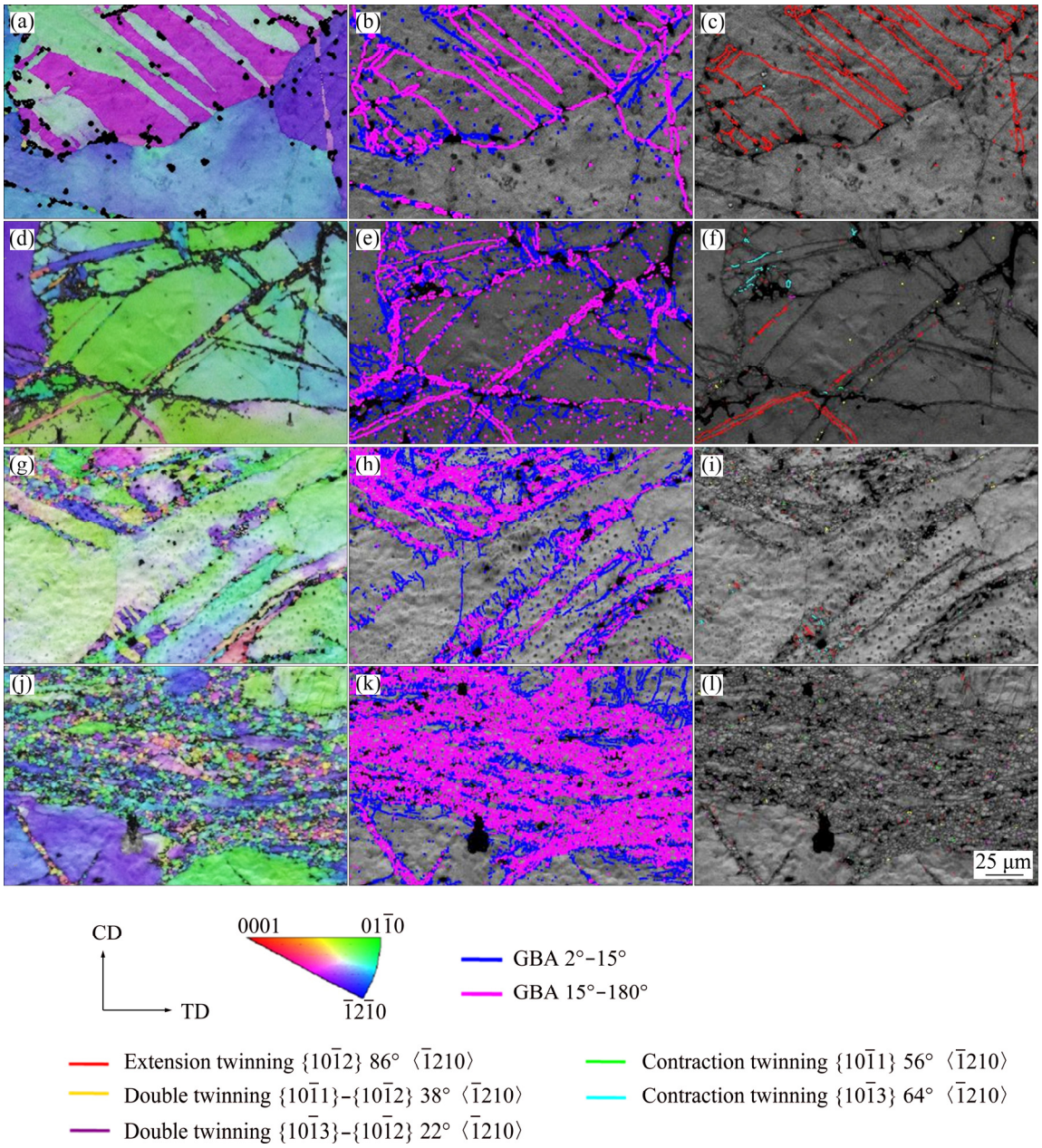

Fig. 8 Inverse pole figures (a, d, g, j), grain boundary angle distribution figures (b, e, h, k) and twin distribution figures (c, f, i, l) of as-compressed alloy at 350 °C with different strains: (a−c) 0.08; (d−f) 0.15; (g−i) 0.45; (j−l) 0.60

occur (as indicated in Figs. 4(b), 4(d) and Fig. 9(d)). The acceleration of DRX via dislocations increment results in the formation of the necklace-like structure around the large primary grains, which further confirms the activation of CDRX mechanism at 350 °C during compression.

3.4 Texture evolutions of Mg−Zn−Er alloy

The texture intensity as well as texture type shows a strong dependence on both temperature and strain. In particular, the texture intensity is sensitive to temperature. Figure 10 shows the pole figures of specimens after compression with different strains. When the temperature is 200 °C, the plastic deformation mainly relies on the basal slip and the pyramidal twin, which leads to a strong texture at a low strain owing to lower deformation temperature, as shown in Figs. 10(a) and (b). The experimental results show that the main texture consists of $\{10\bar{1}0\}\langle 0001\rangle$ and $\{11\bar{2}0\}\langle 0001\rangle$. At the strain of 0.45, the main texture turns into $\{11\bar{2}0\}\langle 10\bar{1}0\rangle$, as indicated in Figs. 10(c) and (d). However, the texture intensity changes little, which is ascribed to the twin-dominant deformation mechanism. When the temperature raises to 350 °C, the texture feature of the specimen shows a significant difference, compared with that at 200 °C. It is observed that the texture component

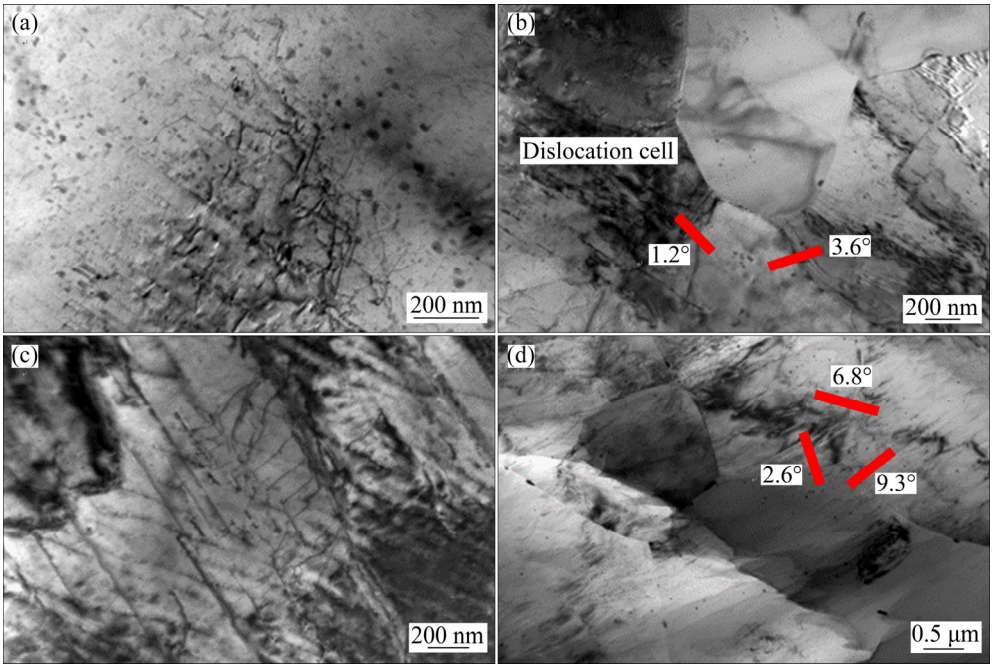

Fig. 9 TEM images of as-compressed alloy at 350 °C with different strains: (a, b) 0.15; (c, d) 0.60

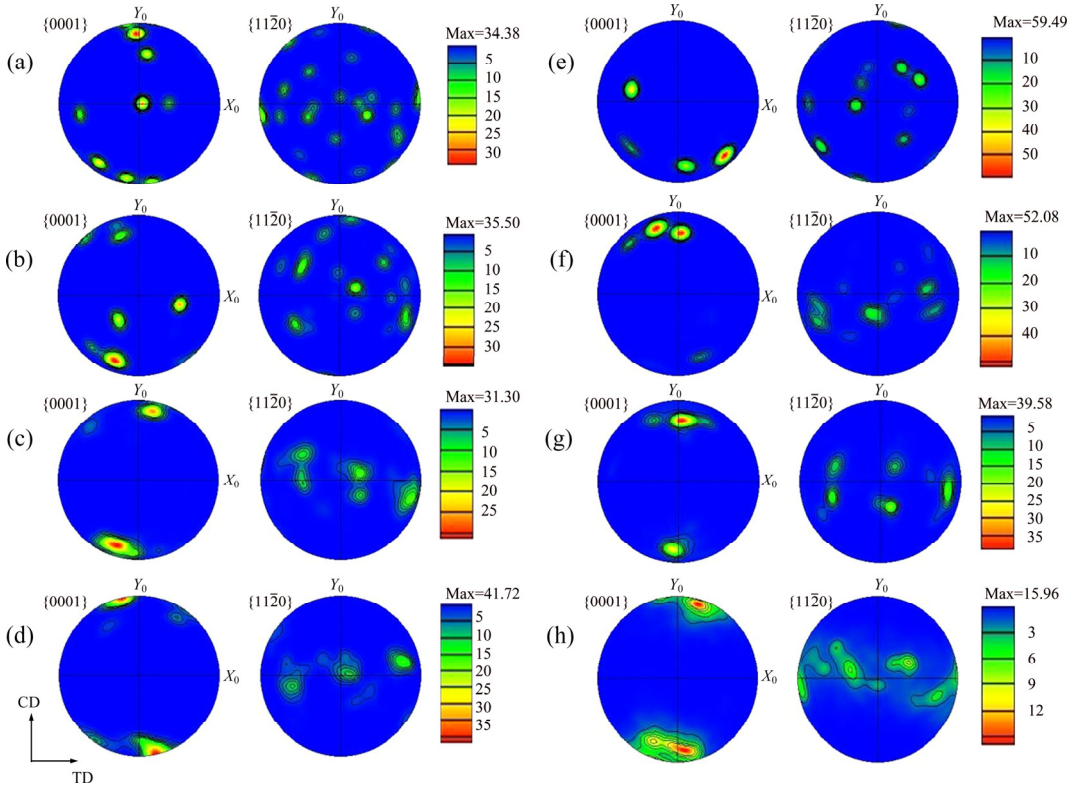

Fig. 10 Pole figures of specimens after compression with different strains at 200 °C (a−d) and 350 °C (e−h): (a, e) 0.08; (b, f) 0.15; (c, g) 0.45; (d, h) 0.60

tilts about 45° from the CD at the strain of 0.08, as shown in Fig. 10(e). The maximum intensity value of the texture is ~59.49, which is far higher than that of the as-compressed specimen at 200 °C, i.e., 34.38. This implies that the decrease in twin intensity is not beneficial to modifying the texture. On the contrary, the twin has an obvious effect on weakening the texture in the initial deformation. The coarse grain structure produces a large number of twins in the process of deformation, which offers a possible means to modify the texture via rotating the basal plane by 86° [30]. With improvement of the strain, the texture component gradually shifts to $\{11\bar{2}0\}\langle 10\bar{1}0\rangle$ texture (Figs. 10(f) and (g)). Ultimately, the texture type is $\{11\bar{2}0\}\langle 0001\rangle$,

as shown in Fig. 10(h). Meanwhile, the texture intensity drops rapidly as the strain increases, which is also ascribed to the CDRX mechanism [1].

3.5 Precipitations of Mg−Zn−Er alloy during compression

Figure 11 shows the bright field TEM images of precipitates in the as-compressed alloy at the strain of 0.6. At 200 °C, there are large amounts of precipitates in both matrix and grain boundaries (Figs. 11(a) and (b)). The dimensions of particles at grain boundaries range 50−100 nm. Furthermore, the corresponding high-resolution TEM (HRTEM) and Fourier transformation (FFT) shows a typical nano-scale icosahedral quasicrystalline phase (*I*-phase, Mg_3Zn_6Er, as seen in Fig. 11(b)) with 3-fold symmetry [31]. Meanwhile, the needle or rod-shaped precipitates with several nanometers in width and 50 nm in length are dispersed in matrix, and they correspond to the Mg−Zn intermetallic phase [32]. However, it is found that the number of nano-scale *I*-phase (in 2-fold symmetry) in matrix increases at 350 °C, as shown in Figs. 11(c) and (d). Also, the nano-scale *I*-phases distribute more uniformly.

Previous investigations have shown that the thermo-mechanical treatment can not only destroy the large-size dendritic *I*-phase, but also promote the formation of a large amount of nano-scale *I*-phase, rendering dispersive distribution in matrix [31,32]. In this work, the deformation mechanisms of the alloy are main basal slip and twinning at 200 °C. Therefore, a considerable amount of deformation twin boundaries act as strong obstacles for dislocations motion, resulting in stress concentration, which leads to the precipitation of the nano-scale *I*-phase at grain boundaries. The stress plays an important role in introducing precipitations of the nano-scale *I*-phase and the Mg−Zn phase at 200 °C. When the deformation temperature is increased to 350 °C, the main precipitates are only the nano-scale *I*-phases. The nano-scale *I*-phases pin and hinder the dislocations motion, which leads to dislocation tangles and dislocation cells (Fig. 11(d)).

As stated above, the temperature is one of the key factors that influence the plastic deformation mechanism of Mg−Zn−Er alloy. The CRSS of non-basal slips and twinning are difficult to be activated compared with the basal slip at room temperature. The twinning and non-basal slips can be started and two competing deformation mechanisms are present when the high stress concentration is caused by inelastic strain. However, the twin nucleation is a process of stress-induced activation rather than heat-induced activation compared with the non-basal slips [29,33]. Therefore, the number of $\langle a+c \rangle$ slip is large at room temperature and drops rapidly as the temperature is increased. Meanwhile, the twinning is expected to be relatively temperature-insensitive. Consequently, when the compression temperature is 200 °C, the twinning always exists in the whole process of the deformation and it is one of the main deformation mechanisms. With the strain of 0.6, the TDRX mechanism starts to happen because of the activation of the non-basal slip. However, the increase of temperature up to 350 °C leads to the activation of the non-basal slip, which results in the occurrence of the CDRX instead of the twins.

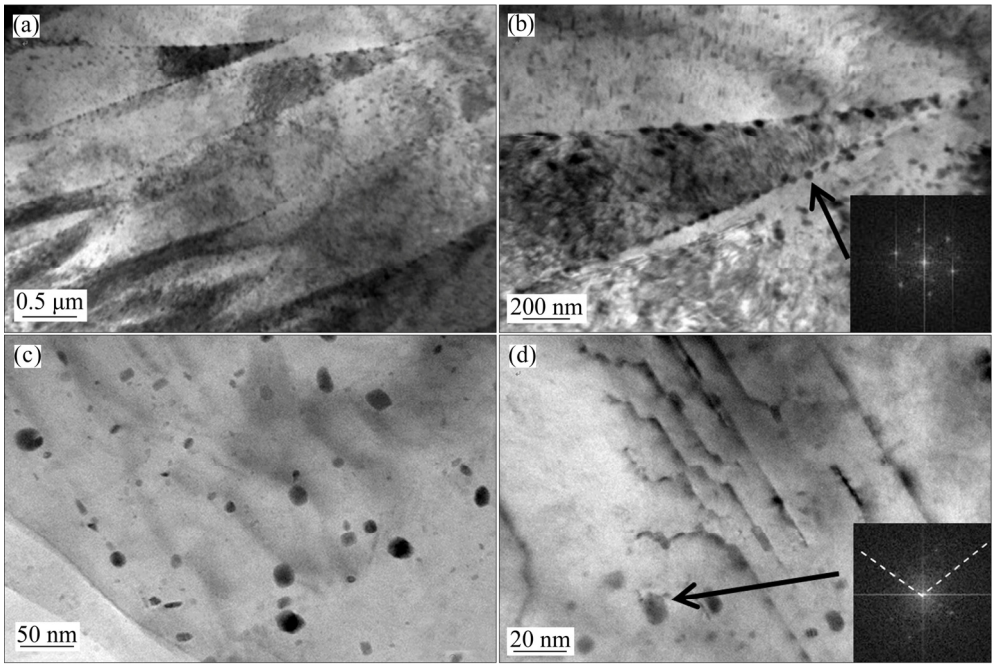

Fig. 11 Bright field TEM images of precipitates of as-compressed alloy with strain of 0.6 at different temperatures: (a, b) 200 °C; (c, d) 350 °C

4 Conclusions

1) The temperature has a great influence on DRX mechanism. At the low temperature of 200 °C, the twinning is one of the main deformation mechanisms during the whole compression process. The TDRX begins to happen at the strain of 0.6 due to the activation of non-basal slips. Ultimately, the dominant features of microstructures are double twins and shear bands. At the high temperature of 350 °C, the twinning is still one of the main deformation mechanisms at a low strain. However, with the increase in deformation degree, CDRX substitutes the twining, and the final microstructure consists of necklace-like structures and initial grains.

2) The twin bands are mainly composed of dislocation walls, second twins, double twins, and micro-twins. These fine second twins are nuclei of TDRX. The shear begin began to form as the twin bands are consumed by ultrafine TDRX grains because of the activation of non-basal slips.

3) In the initial deformation stage, more tension twins result in the weaker texture. As the strain is increased, the increase in numbers of DRX grains noticeably decreases the texture at 350 °C. In addition, some kinds of nano-scale second phases precipitate during the deformation. The new precipitates of Mg−Zn binary phase and nano-sale *I*-phases are observed at 200 °C. The nano-scale *I*-phases are found as main precipitates during deformation at 350 °C.

References

[1] WANG Qing-feng, DU Wen-bo, LIU ke, WANG Zhao-hui, LI Shu-bo, WEN kai. Microstructure, texture and mechanical properties of as-extruded Mg−Zn−Er alloys [J]. Materials Science and Engineering A, 2013, 581: 31−38.

[2] HANTZSCHE K, BOHLEN J, WENDT J, KAINER K U, YI S B, LETZIG D. Effect of rare earth additions on microstructure and texture development of magnesium alloy sheet [J]. Scripta Materialia, 2010, 63: 725−730.

[3] WU Luo-yi, LI Hao-tian, YANG Zhong. Microstructure evolution during heat treatment of Mg−Gd−Y−Zn−Zr alloy and its low-cycle fatigue behavior at 573 K [J]. Transactions of Nonferrous Metals Society of China, 2017, 27: 1026−1035.

[4] ANDO D, KOIKE J, SUTOU Y. Relationship between deformation twinning and surface step formation in AZ31 magnesium alloys [J]. Acta Materialia, 2010, 58: 4316−4324.

[5] GALIVEV A, KAIBYSHEV R, GOTTSTEIN G. Correlation of plastic deformation and dynamic recrystallization in magnesium alloy ZK60 [J]. Acta Materialia, 2001, 49: 1199−1207.

[6] SITDIKOV O, KAIBYSHEV R. Dynamic recrystallization in pure magnesium [J]. Materials Transactions, 2001, 42: 1928−1937.

[7] XU S W, KAMADO S, MATSUMOTO N, HONMA T, KOJIMA Y. Recrystallization mechanism of as-cast AZ91 magnesium alloy during hot compressive deformation [J]. Materials Science and Engineering A 2009, 527: 52−60.

[8] FU H, GE B C, XIN Y C, WU R Z, FERNANDEZ C, HUANG J Y, PENG Q M. Achieving high strength and ductility in magnesium alloys via densely hierarchical double contraction nano twins [J]. Nano Lett, 2017, 17: 6117−6124.

[9] LI X, YANG P, WANG L N, MENG L, CUI F. Orientational analysis of static recrystallization at compression twins in a magnesium alloy AZ31 [J]. Materials Science and Engineering A, 2009, 517: 160−169.

[10] SU J, SANIARI M, KABIR A S H, JUNG I H, YUE S. Dynamic recrystallization mechanisms during high speed rolling of Mg−3Al−2Zn alloy sheets [J]. Scripta Materialia, 2016, 113: 198−201.

[11] KIM K H, SUH B C, BAE J H, SHIM M S, KIM S, KIM N J. Microstructure and texture evolution of Mg alloy during twin-roll casting and subsequent hot rolling [J]. Scripta Materialia, 2010, 63: 716−720.

[12] XU S W, ZHENG M Y, KAMADO S, WU K, WANG G J, LV X Y. Dynamic microstructural changes during hot extrusion and mechanical properties of a Mg−5.0Zn−0.9Y−0.16Zr (wt.%) alloy [J]. Materials Science and Engineering A, 2011, 528: 4055−4067.

[13] BASU I, Al-SAMMAN T. Twin recrystallization mechanisms in magnesium-rare earth alloys [J]. Acta Materialia, 2015, 96: 111−132.

[14] SUN Cui-cui, LIU Ke, WANG Zhao-hui, LI Shu-bo, DU Xian, DU Wen-bo. Hot deformation behaviors and processing maps of Mg−Zn−Er alloys based on Gleeble−1500 hot compression simulation [J]. Transactions of Nonferrous Metals Society of China, 2016, 26: 3123−3134.

[15] JIANG L, JONAS J J. Effect of twinning on the flow behavior during strain path reversals in two Mg (+Al, Zn, Mn) alloys [J]. Scripta Materialia, 2008, 58: 803−806.

[16] HONG S G, PARK S H, LEE C S. Role of $\{10\bar{1}2\}$ twinning characteristics in the deformation behavior of a polycrystalline magnesium alloy [J]. Acta Materialia, 2010, 58: 5873−5885.

[17] XIAO Hong-chao, JIANG Shu-nong TANG Bei, HAO W H, GAO Yong-hao, CHEN Zhi-yong, LIU Chu-ming. Hot deformation and dynamic recrystallization behaviors of Mg−Gd−Y−Zr alloy [J]. Materials Science and Engineering A, 2015, 628: 311−318.

[18] GAO L, LUO A A. Hot deformation behavior of as-cast Mg−Zn−Mn−Ce alloy in compression [J]. Materials Science and Engineering A, 2013, 560: 492−499.

[19] JIANG L, JONAS J J, MISHRA R K, LUO A A, SACHDEV A K, GODET S. Twinning and texture development in two Mg alloys subjected to loading along three different strain paths [J]. Acta Materialia, 2007, 55: 3899−3910.

[20] MEYERS M A, VOHRINGER O, LUBARDA V A. The onset of twinning in metals: A constitutive description [J]. Acta Materialia, 2001, 49: 4025−4039.

[21] BARNETT M R, KESHAVARZ Z, BEER A G, ATWELL D. Influence of grain size on the compressive deformation of wrought Mg−3Al−1Zn [J]. Acta Materialia, 2004, 52: 5093−5103.

[22] BARNETT M R, NAVE M D, BETTLES C J. Deformation microstructures and textures of some cold rolled Mg alloys [J]. Materials Science and Engineering A, 2004, 386: 205−211.

[23] COULING S L, PASHAK J F, STURKEY L. Unique deformation and aging characteristics of certain magnesium-base alloys [J]. American Social Metal Transaction, 1959, 51: 94−107.

[24] WANG Yan-nan, XIN Yun-chang, YU Hui-hui, LV Liang-chen, LIU Qing. Formation and microstructure of shear bands during hot rolling of a Mg−6Zn−0.5Zr alloy plate with a basal texture [J]. Journal of Alloys and Compounds, 2015, 644: 147−154.

[25] YIN D L, ZHANG K F, WANG G F, HAN W B. Warm deformation behavior of hot-rolled AZ31 Mg alloy [J]. Materials Science and Engineering A, 2005, 392: 320−325.

[26] SITDIKOV O, KAIBYSHEV R, SAKAI T. Dynamic

recrystallization based on twinning in coarse-grained Mg [J]. Materials Science Forum, 2003, 419: 521−526.

[27] del VALLE J A, PE´REZ-PRADO M T, RUANO O A. Texture evolution during large-strain hot rolling of the Mg AZ61 alloy [J]. Materials Science and Engineering A, 2003, 355: 68−78.

[28] TAN J C, TAN M J. Dynamic continuous recrystallization characteristics in two stage deformation of Mg−3Al−1Zn alloy sheet [J]. Materials Science and Engineering A, 2003, 339: 124−132.

[29] SAKAI T, BELYAKOV A, KAIBYSHEV R, MIURA H, JONAS J J. Dynamic and post-dynamic recrystallization under hot, cold and severe plastic deformation conditions [J]. Progress of Materials Science, 2014, 60: 130−207.

[30] XIN Yun-chang, WANG Mao-yin, ZENG Zhen, HUANG Guang-jie, LIU Qing. Tailoring the texture of magnesium alloy by twinning deformation to improve the rolling capability [J]. Scripta Materialia, 2011, 64: 986−989.

[31] MEDINA J, PÉREZ P, GARCES G, TOLNAI D, STARK A, SCHLL N, ADEVA P. Microstructural changes in an extruded Mg−Zn−Y alloy reinforced by quasicrystalline *I*-phase by small additions of calcium, manganese and cerium-rich mischmetal [J]. Materials Characterization, 2016, 118: 186−198.

[32] HUANG Hua, TIAN Yuan, YUAN Guang-yin, CHEN Chun-lin, DING Wen-jing, WANG Zhong-chang. Formation mechanism of quasicrystals at the nanoscale during hot compression of Mg alloys [J]. Scripta Materialia, 2014, 78−79: 61−64.

[33] NAVE M D, BARNETT M R. Microstructures and textures of pure magnesium deformed in plainest rain compression [J]. Scripta Materialia, 2004, 51: 881−885.

热压缩过程中温度对 Mg−Zn−Er 合金显微组织及织构演化的影响

刘金学[1]，刘 轲[1]，杜文博[1]，李淑波[1]，王朝辉[1]，杜 宪[1]，孙翠翠[2]

1. 北京工业大学 材料科学与工程学院，北京 100124；
2. 山东科学院，济南 250014

摘 要：通过光学显微镜、场发射扫描电镜和透射电镜研究热压缩过程中 Mg−Zn−Er 合金的显微组织及织构的演化。结果表明，温度对动态再结晶(DRX)具有很大的影响。当温度为 200 °C、应变量为 0.6 时，由于应力集中使得非基面滑移⟨*a*+*c*⟩位错被激活，孪生动态再结晶机制(TDRX)开始启动。当温度为 350 °C 时，围绕着初始晶粒的项链状结构出现，这是典型的连续动态再结晶机制(CDRX)。动态再结晶对弱化织构具有非常重要的影响，同时低温下孪生对弱化织构也起到一定的作用。研究还发现，当温度从 200 °C 提高到 350 °C 时，由于动态再结晶形核位点从孪晶界向初始晶界转移，织构减弱。

关键词：Mg−Zn−Er 合金；热压缩；动态再结晶；孪生；织构

(Edited by Bing YANG)